Journal of Hip Preservation Surgery, 2025, **12**, 65–73
DOI: https://doi.org/10.1093/jhps/hnae048
Advance access publication date: 25 December 2024
Research Article

The ability of plain radiography to accurately describe the bone surface at the head–neck junction of the femur: a study using human bone models

Tomohiro Mimura*, Yuki Furuya, Kosuke Kumagai, Yasutaka Amano, Shunichi Miyahara, Ryota Uemura, Sadafumi Horikawa, Hideki Saito, Kohei Umeda, Fumitaka Ushiyama, Yugen Ogata, Takafumi Yayama, Kanji Mori, Shinji Imai

Department of Orthopedic Surgery, Shiga University of Medical Science, Tsukinowa-cho, Seta, Otsu, Shiga 520-2192, Japan

*Corresponding author. Department of Orthopedic Surgery, Shiga University of Medical Science, Tsukinowa-cho, Seta, Otsu, Shiga 520-2192, Japan.
E-mail: tmimura@belle.shiga-med.ac.jp

ABSTRACT

In evaluations of a cam deformity on femoroacetabular impingement, the head–neck junction (HNJ) must be accurately assessed. We conducted this study to determine the ability of plain radiography to visualize the end-to-end bone surface of the HNJ. We used six human bone models. Ten examiners evaluated the degree to which attached stainless wire marker at the 1:00, 1:30, and 2:00 radial plane defined in reconstructed computed tomography can be accurately detected on the bone surface on plain radiographies. We employed 13 plain radiographies: the cross-table lateral view, frog-leg lateral view, Espié frog-leg lateral view, false-profile view, modified false-profile view, 30° Dunn view (DV), 45° DV, 60° DV, 90° DV, 30° modified Dunn view (MDV), 45° MDV, 60° MDV, and 90° MDV. Examiners scored the degree to which the radiographic images accurately detected the stainless wire marker on the bone surface of the HNJ on a scale of 1 point (0% match) to 5 points (almost 100% match). The highest score for the 1:00 plane was 4.98 points on the 45° DV. Similarly, the highest scores of the 1:30 and 2:00 planes were 4.98 points for the 45° MDV and 4.68 points for the 90° MDV, respectively. On these bone model studies, the most suitable plain radiography for describing the HNJ at the 1:00, 1:30, and 2:00 planes were both the 45° DV, the 45° MDV, and the 90° MDV, respectively.

INTRODUCTION

Femoroacetabular impingement (FAI) was recently reported as a cause of osteoarthritis of the hip [1, 2]. For an accurate determination of the position and the degree of a cam deformity in a patient with FAI, it is necessary to evaluate the head–neck junction (HNJ) in the anterosuperior radial plane and/or three-dimensionally [3–6]. Therefore, we usually evaluate this deformity with computed tomography (CT) and/or magnetic resonance imaging (MRI). However, CT has a definite issue of high radiation exposure and high-quality MRI is not available throughout the world. Several reports suggest that it is important to evaluate a cam deformity from the 1:00 plane to the 2:00 plane on the reconstructed radial plane (on the right side) [5, 7–9], and several reports using simulation with CT data have demonstrated that the pinpoint evaluation for the transition part of the HNJ on these planes could be visualized using several plain radiographies [10, 11]. We thus hypothesized that plain radiographies can describe not only the transition part of HNJ but also the longitudinal bone surface along the width of the HNJ, on these important planes. We conducted the present study to investigate the ability of plain radiography to describe the end-to-end bone surface of the HNJ on the 1:00, 1:30, and 2:00 planes, using real bone models.

MATERIALS AND METHODS

We used six human bone models maintained in division of Anatomy and Cell Biology, Department of Anatomy, Shiga University of Medical Science. We randomly selected the human bone model (pelvis and femur) from the several dozen collection box. Exclusion criteria were (i) massively damaged bones, (ii) clearly small specimen, (iii) damaged bone models at bone surface between the middle point of the femoral neck and the central plane of the femoral head, (iv) macroscopically defect or damaged bones at distal femoral condyle and lesser trochanter. The requirement for study approval was waived by our institution's ethics committee because no humans were involved.

Received 9 November 2023

Table 1. Morphogenetic feature of femoral bone models

Bone model	#1	#2	#3	#4	#5	#6	Average ± SD (range) [95% confidence interval]
Length of the femur (mm)	38	41	36	38	44	38	39.2 ± 5.4 (36–44) [34.8–43.5]
Femoral head diameter (mm)	42.1	45.0	42.2	42.0	48.6	46.7	44.4 ± 5.1 (42.1–48.6) [40.3–48.5]
Femoral neck-shaft angle (°)	128.8	131.3	132.4	124.2	130.1	134.0	130.1 ± 6.0 (124.2–134.0) [125.4–134.9]
Femoral neck anteversion[a] (°)	7.8	23.6	12.7	14.7	12.3	15.3	14.4 ± 10.0 (7.8–23.6) [6.4–22.4]
α-angle[b] (°)	44.3	43.0	52.4	43.2	52.1	50.7	47.6 ± 8.5 (43.2–52.1) [40.8–54.4]
Head–neck offset[b] (mm)	5.9	5.8	5.1	9.1	7.6	5.9	6.6 ± 2.8 (5.1–9.1) [4.3–8.8]
Head–neck offset ratio[b]	0.14	0.129	0.118	0.217	0.153	0.126	0.147 ± 0.07 (0.12–0.22) [0.09–0.20]

[a]Femoral neck anteversion was evaluated from the transcondylar plane on the CT axial image.
[b]α-angle, head–neck offset, and head–neck offset ration were evaluated on the reconstructed 1:30 radial plane on the CT image.

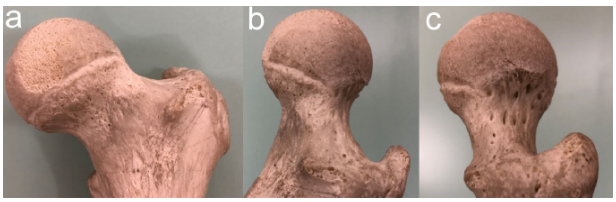

Figure 1. The macroscopic findings of the proximal part of the left femur of a representative human bone model (model #1). (a) Anterior, (b) anterosuperior, and (c) superior views.

Figure 2. An anteroposterior pelvic radiographic image of a representative bone model (model #1), which has no pistol grip deformity at the HNJ of the left femur, and the femoral neck-shaft angle is 128.8°.

The anatomical features of the bone models

Table 1 provides the bone morphogenetic features of six femoral bone models that met the exclusion criteria; namely, no massively bone damage, adult size, and especially no damage on the HNJ, distal femoral condyle, and lesser trochanter. Figure 1 provides a macroscopic photograph of the proximal part of the representative bone model (model #1), and Fig. 2 shows an anteroposterior pelvic radiography of these representative models.

The methods for reconstructing each radial plane using CT

Each left femur was put on the table of the CT system. The line connecting the center of the femoral head and the center of the distal femoral condyle was set parallel to the sagittal plane (no abduction). In addition, the plane connecting the bilateral posterior femoral condyle and the posterior facet of the greater trochanter was set parallel to the coronal plane (no flexion), and the transcondylar line was also set parallel to the coronal plane (no rotation). Axial and sequential CT images were obtained without a gantry tilt (120 kV, 160 mA, 0.5 s) using a Toshiba Aquilion CX system (Toshiba Medical Systems, Tokyo). CT was taken at 0.313 mm in axial slice (the slice thickness was 0.625 mm), and the volume was approximately 1150 to 1400 images on axial slice. The data were reconstructed under conditions suitable for a bone evaluation using AquariusNET Viewer software (TeraRecon, San Francisco, CA). This software enables reconstructions of optimal sagittal, coronal, and axial planes as well as three-dimensional reconstructed CT images. In the present study, the multiple radial planes of the left femur were reconstructed as described [4, 12]. The 2:00 radial plane was rotated superiorly by 30° on the oblique axial slice. Similarly, the 1:30 radial plane was rotated superiorly by 45° on the oblique axial slice, and the 1:00 radial plane was rotated superiorly by 60° on the oblique axial slice (Fig. 3). The solid plane in the dotted cut line in Fig. 3a corresponds to the vertical line in Fig. 3b. The plane rotated 30 degrees, 45 degrees, and 60 degrees upward along the solid line (femoral neck axis) in Fig. 3a corresponds to the 2:00 radial plane, 1:30 radial plane, and 1:00 radial plane shown in Fig. 3b, respectively.

The accurate identification of the HNJ on each radial plane

We attached stainless 0.45 mm-diameter stainless wire markers on the bone surface between the middle point of the femoral neck and the central level of the femoral head with clear tape on each radial plane and then performed CT imaging. Until the wire markers were uniformly and completely matched to the HNJ; namely, bone surface from the middle point of the femoral neck (point X in Fig. 4a) to the central level of the femoral head (point Y in Fig. 4a), we took CT images while adjusting the positions and the lengths of the stainless wire markers over and over again on every 1:00, 1:30, and 2:00 planes. With this protocol, we identified the HNJ on these models at the 1:00, 1:30, and 2:00 radial planes, respectively (Fig. 4).

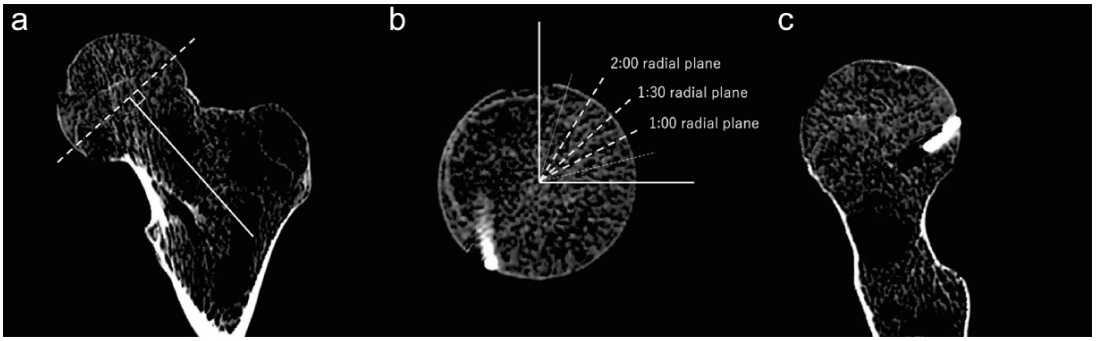

Figure 3. The methods for reconstructing each radial plane. (a) The oblique-coronal plane reconstructed on true femoral neck axis. *Solid line*: The axis of the femoral neck through the femoral head center. *Dotted line*: The reference plane for radial angle reconstruction. (b) The reconstructed oblique-axial plane (plane on dotted line of A). The reconstructed plane shows a superimposed radial reference line. The radial planes reconstructed from each dotted line are the 1:00, 1:30, and 2:00 radial planes. (c) The reconstructed radial plane (oblique-sagittal plane). The 2:00 radial plane is demonstrated in this figure.

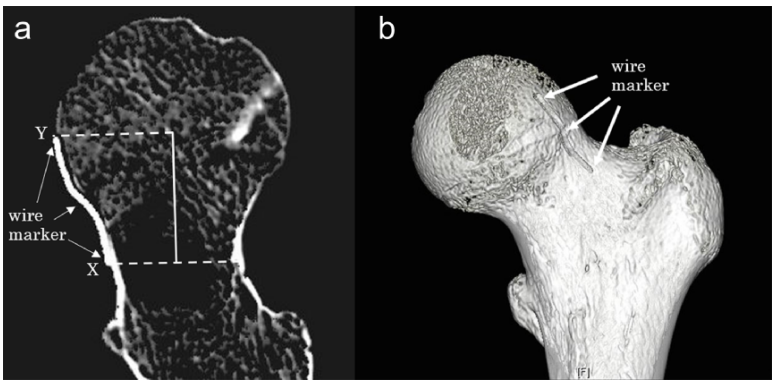

Figure 4. Definition of the HNJ of radial planes. In this study, the part indicated by the middle arrow was expressed as the transition part of HNJ. (a) The *solid line* is the line connecting the femoral head center and the middle point of the femoral neck isthmus. The *dotted line* is the perpendicular line from the femoral head center and middle point of the femoral neck. The anterior bone surface from the middle point of the femoral neck to the center plane of the femoral head, sandwiched between these perpendicular lines (from point X to point Y), is the HNJ. We adjusted the position and the length of the stainless wire markers until they were uniformly detected on the bone surface. In this image, the HNJ of the 1:30 plane identified with a stainless wire marker was revealed. (b) Visual image of the HNJ of the 1:30 plane. The HNJ on the 1:30 plane is demonstrated here on reconstructed anteroposterior 3DCT image.

Table 2. Femoral position for each radiographic view

	Abduction	Flexion	External rotation
Cross-table lateral view	0	0	−15
Frog-leg lateral view	45	0	60
Espié frog-leg lateral view	45	45	30
False-profile view	0	0	90
Modified false-profile view	0	0	55
30° DV	20	30	0
45° DV	20	45	0
60° DV	20	60	0
90° DV	20	90	0
30° MDV	20	30	40
45° MDV	20	45	40
60° MDV	20	60	40
90° MDV	20	90	40

The data are degrees (°).

Evaluate the radiographic view in which the marker can be detected to overlap the radiographic cortical line of the HNJ

We examined 13 plain radiography images (Table 2). We controlled the femoral position on each radiography image as follows. First, the abduction angle was controlled by the angle between the line connecting the femoral head and the middle point of the distal condyles and the sagittal plane. Next, the internal–external rotation angle was controlled by the angle between the posterior condylar line and the coronal plane. Finally, the flexion angle was controlled by the angle between the line connecting the posterior facet of the greater trochanter posterior and the posterior facet of the distal condyle (the posterior facet of the lateral condyle was used if the femur was set in external rotation) and the coronal plane. An orthopaedic surgeon (T.M.) wearing full X-ray protection controlled the femoral angle, and each radiographic image was taken only once in each of the 1:00, 1:30, and 2:00 planes.

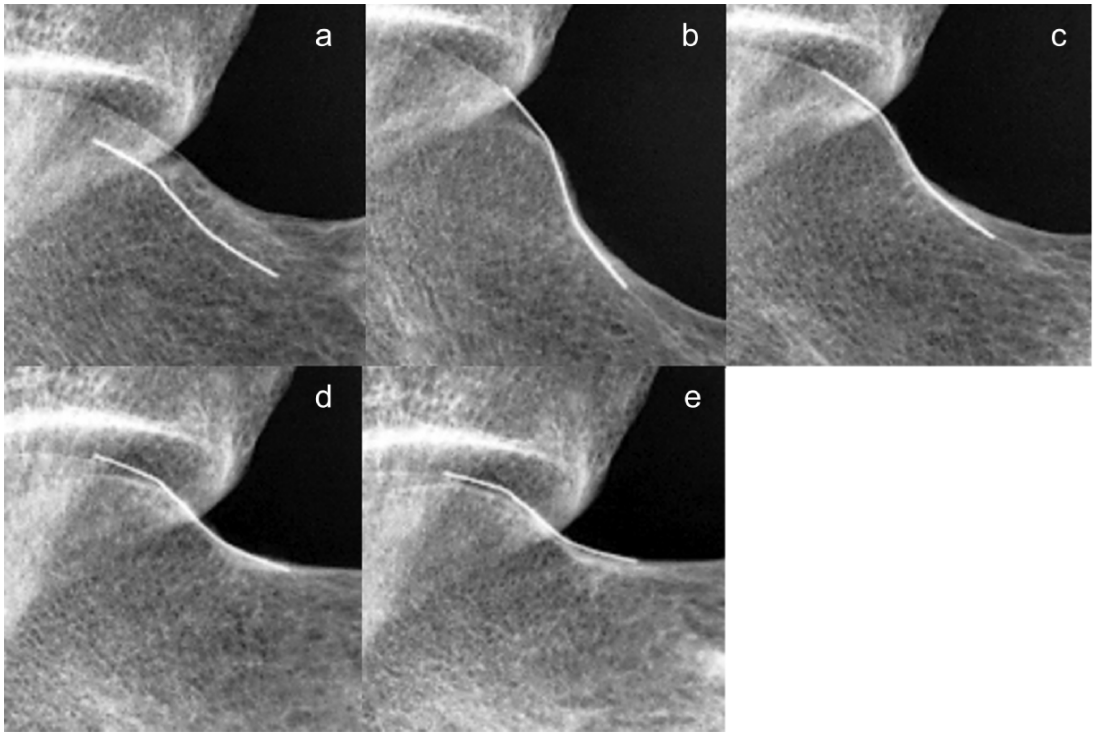

Figure 5. Representative cases (model #1) of the degree to which the stainless wire markers could be accurately detected on the end-to-end bone surface of head-neck junction (HNJ). (a) 1 point: The stainless wire marker and the bone surface are 0% match. (b) 2 points: The stainless wire marker and bone surface are less than 50% match. In this case, the markers were detected on the bone surface only around the femoral head side. (c) 3 points: The stainless wire marker and bone surface are almost 50% match. In this case, the markers were detected on the bone surface from the femoral head to the transition part of HNJ. (d) 4 points: The stainless wire marker and bone surface are more than 50% match. In this case, the marker at the middle point of the fmoral neck was incompletely detected on the bone surface. (e) 5 points: The stainless wire marker and bone surface are almost 100% match. In this case, the markers and bone surface are an almost complete match at the end-to-end bone surface of HNJ.

On the Espié frog-leg lateral view (EFLV) [13], the Dunn view (DV), and the modified Dunn view (MDV), conventional anteroposterior pelvic radiography was used [14]. The X-ray tube-to-film distance was 120 cm, with the tube oriented perpendicular to the table. The crosshairs of the beam were centered on the point midway between the superior border of the pubic symphysis and a line drawn connecting the anterior superior iliac spine. Referring to the conventional 45° DV and 90° DV [14, 15], the flexion angle of the 30° DV and 60° DV were changed to 30° and 60°, respectively. Similarly, referring to the conventional 45° MDV [14, 15], the flexion angle of the 30° MDV, 60° MDV, and 90° MDV were changed to 30°, 60°, and 90°, respectively.

The cross-table lateral view was taken with 15° internal rotation, and the center of the crossfire of the beam was set to the femoral head as described for clinical settings [14]. The frog-leg lateral view was taken unilaterally, and the crosshairs of the beam were directed at a point midway between the anterior superior iliac spine and the pubic symphysis of the left hip [14]. The false-profile view (FPV) was taken in 0° abduction, 0° flexion, and 90° external rotation with the crosshairs of the beam set to the femoral head, referring to the conventional standing method [14, 16]. In this FPV, the pelvis was rotated to the left in order to avoid impingement between the femoral HNJ and the acetabulum. The modified false-profile view was taken in 0° abduction, 0° flexion, and 55° external rotation referring to the report from Atkins *et al.* [10].

Ten examiners who were blinded to the radiography protocol and the evaluated radial plane examined the degree to which the stainless wire markers were accurately detected to overlap the radiographic cortical line of the HNJ at the 1:00, 1:30, and 2:00 planes; they subjectively scored the accuracy on a scale of 1 to 5 points as illustrated in Fig. 5: 1 point = the stainless wire marker and the bone surface was 0% match; 2 points = the stainless wire marker and bone surface was less than 50% match; 3 points = the stainless wire marker and bone surface was almost 50% match; 4 points = the stainless wire marker and bone surface was more than 50% match; and 5 points = the stainless wire marker and bone surface was almost 100% match. Each examiner performed three sets of assessment at 1 week intervals.

Statistical analyses

Wilcoxon signed-rank test was employed to determine the statistical significance between the best radiographic limb position over the other radiographic limb positions on each plane. Value of $P < .05$ was considered to indicate statistical significance. To determine the intra- and interobserver reliability correlations of the scores, we calculated the intraclass correlation coefficients (ICCs). The intraobserver and interobserver reliability were evaluated using the results of the all examiners' three

Table 3. Average score of each radiograph on the 1:00 plane (60° radial plane)

Bone model:	**#1**	**#2**	**#3**	**#4**	**#5**	**#6**	**In total average ± SD**
Cross-table lateral view	1.63	1.00	1.00	1.00	1.03	1.00	1.11 ± 0.22
Frog-leg lateral view	1.17	1.00	1.27	1.13	1.03	1.00	1.10 ± 0.09
Espié frog-leg lateral view	4.83	3.57	4.93	1.60	4.97	4.00	3.98 ± 1.10
False-profile view	1.00	1.00	1.00	1.00	1.00	1.00	1.00 ± 0.00
Modified false-profile view	1.07	1.10	1.87	1.57	1.00	1.57	1.36 ± 0.30
30° DV	4.00	4.97	5.00	5.00	4.97	4.97	4.82 ± 0.34
45° DV	4.90	4.97	5.00	5.00	5.00	5.00	4.98 ± 0.03
60° DV	4.90	4.27	4.97	4.80	5.00	3.87	4.63 ± 0.39
90° DV	2.80	2.63	1.10	1.00	2.93	1.00	1.91 ± 0.82
30° MDV	3.33	1.40	2.17	1.03	2.37	1.33	1.94 ± 0.72
45° MDV	2.13	1.83	2.53	1.03	2.27	1.27	1.84 ± 0.50
60° MDV	1.77	1.93	2.00	1.00	2.80	1.00	1.75 ± 0.58
90° MDV	1.00	1.00	1.00	1.00	1.83	1.00	1.14 ± 0.27

The data are the average score of three examinations by each examiner and are rounded off to the second decimal place.

Table 4. Average score of each radiograph on the 1:30 plane (45° radial pane)

Bone model:	**#1**	**#2**	**#3**	**#4**	**#5**	**#6**	**In total average ± SD**
Cross-table lateral view	2.07	1.17	1.93	1.00	1.83	1.00	1.50 ± 0.42
Frog-leg lateral view	2.60	1.07	2.27	1.17	2.00	1.67	1.79 ± 0.51
Espié frog-leg lateral view	4.00	1.07	5.00	3.60	4.43	5.00	3.85 ± 1.24
False-profile view	1.03	1.00	1.07	1.00	1.00	1.00	1.02 ± 0.02
Modified false-profile view	2.53	1.10	2.27	1.63	2.37	1.77	1.94 ± 0.50
30° DV	2.47	1.47	1.03	2.23	1.00	1.73	1.66 ± 0.52
45° DV	3.00	3.50	2.67	4.90	1.03	3.60	3.12 ± 1.08
60° DV	4.47	4.93	4.97	4.97	2.20	4.97	4.42 ± 0.93
90° DV	3.60	4.33	4.27	3.80	3.60	3.90	3.92 ± 0.27
30° MDV	3.93	4.00	5.00	4.97	3.80	4.90	4.43 ± 0.49
45° MDV	4.93	4.97	5.00	5.00	4.97	5.00	4.98 ± 0.02
60° MDV	4.07	3.67	5.00	3.90	5.00	4.23	4.31 ± 0.48
90° MDV	2.30	2.90	3.97	2.20	2.80	2.07	2.71 ± 0.59

The data are the average score of three examinations by each examiner and are rounded off to the second decimal place.

measurements of each plane on a representative model. The ICC was interpreted using the categories of agreement suggested by Landis and Koch [17], where ≤0.40 is unacceptable, 0.41–0.60 is moderate, 0.61–0.80 is substantial, and ≥0.80 is almost perfect agreement.

RESULTS

The average scores of 3 examinations by 10 examiners for each bone model are provided in Tables 3–5. The most favorable radiographic images for describing the bone surface of the HNJ of the 1:00 plane was the 45° DV (4.98 ± 0.03 points). Similarly, the best image for 1:30 plane was the 45° MDV (4.98 ± 0.02 points), and the best image for the 2:00 plane was the 90° MDV (4.68 ± 0.33 points). The average scores of three examinations of six bone models for each examiner are shown in Figs 6–8 in a line graph. The comparison between the best 45° DV and the second-best 30° DV on 1:00 plane using the average scores obtained for each bone model was not statistically significant ($P = .250$), while the same comparison using the average scores obtained for each examiner was statistically significant ($P = .002$). Similarly, the comparison between the best 45° MDV and the second-best 30° MDV on 1:30 plane using the average scores obtained for each bone model was not statistically significant ($P = .063$), while the same comparison using the average scores obtained for each examiner was statistically significant ($P = .002$). Again, the comparison between the best 90° MDV and the second-best 60° MDV on 2:00 plane using the average scores obtained for each bone model was not statistically significant ($P = .625$), while the same comparison using the average scores obtained for each examiner was statistically significant ($P = .004$).

Table 6 showed the ICCs for the intraobserver reliability of all planes on a representative model. Table 7 showed the ICCs for the interobserver reliability of all planes on a representative model. All of inter- and intraobserver reliability were over 0.93.

DISCUSSION

In this study using human bone models, plain radiography showed differing degrees of accuracy for describing the bone surface of the HNJ, defined by reconstructed CT radial images. Our results indicated that the best plain radiography for describing the HNJ at the 1:00, 1:30, and 2:00 planes was the 45° DV, the 45° MDV, and the 90° MDV, respectively.

Table 5. Average score of each radiograph on the 2:00 plane (30° radial plane)

Bone model:	#1	#2	#3	#4	#5	#6	In total average ± SD
Cross-table lateral view	4.20	2.23	3.87	2.00	4.10	2.33	3.12 ± 0.88
Frog-leg lateral view	2.33	1.73	1.93	1.47	2.13	2.47	2.01 ± 0.32
Espié frog-leg lateral view	2.93	3.00	1.03	3.47	2.87	3.17	2.74 ± 0.73
False-profile view	1.00	1.00	1.00	1.00	1.00	1.00	1.00 ± 0.00
Modified false-profile view	2.23	2.20	1.53	1.87	2.10	2.33	2.04 ± 0.25
30° Dunn view	1.00	1.00	1.00	1.00	1.00	1.07	1.01 ± 0.02
45° Dunn view	1.00	1.00	1.00	1.00	1.10	1.03	1.02 ± 0.03
60° Dunn view	2.40	1.27	1.10	1.10	1.27	1.77	1.48 ± 0.43
90° Dunn view	4.90	4.97	2.67	5.00	3.40	5.00	4.32 ± 0.87
30° MDV	2.97	3.70	1.60	3.97	3.03	4.63	3.32 ± 0.88
45° MDV	4.13	4.20	1.83	4.10	3.13	4.90	3.72 ± 0.91
60° MDV	5.00	5.00	2.67	4.40	3.93	5.00	4.33 ± 0.78
90° MDV	3.93	5.00	4.87	4.93	4.70	4.67	4.68 ± 0.33

The data are the average score of three examinations by each examiner and are rounded off to the second decimal place.

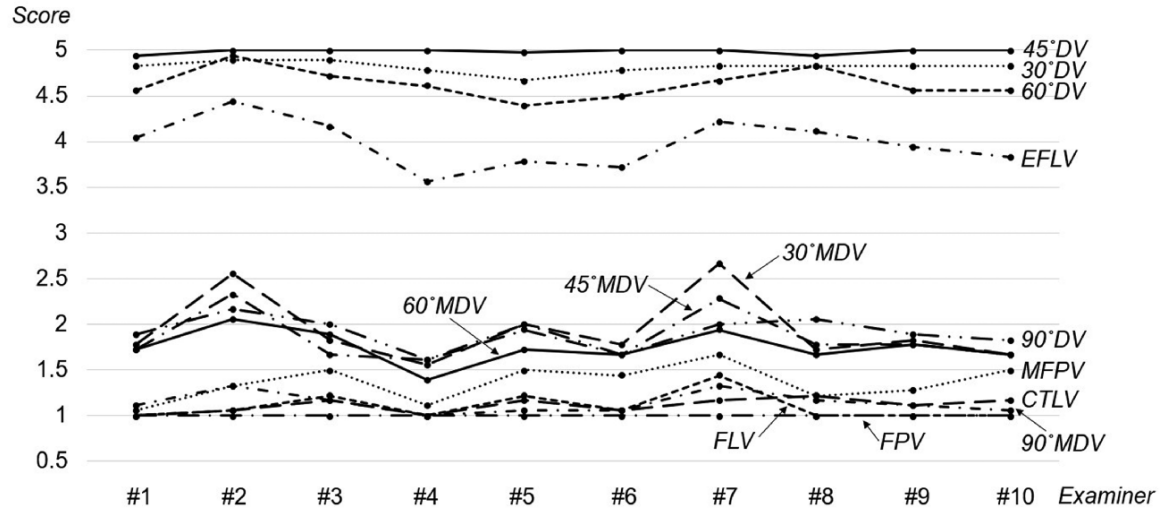

Figure 6. Line graphs showing the examiner's scores on the 1:00 plane. CTLV: cross-table lateral view. The scores are average of 18 measurements, with 3 measurements taken from 6 bone models. 45° Dunn view is the best radiographic image and all examiners give the highest score.

Several research groups have reported the suitability of plain radiography to detect cam deformities [6, 10, 12, 18]. For example, Uemura *et al.* investigated which parts of the HNJ can be described by plain radiography, using a 3D surface model adjusted to the neutral position from patients' CT data [12]. They reported that the EFLV showed the 2:14 plane of the HNJ and the 45° MDV showed the 2:35 plane of the HNJ. However, these reports were pinpoint evaluation for transition part of the HNJ, and to the best of our knowledge, there has been no reports that evaluate the longitudinal bone surface along the width of the HNJ, which had a certain length between the middle point of the femoral neck and the central level of the femoral head. Furthermore, there has been no report of a method that can be used to determine the degree to which the end-to-end bone surface of the HNJ can be described by plain radiography. We thus conducted an investigation of how radiography images can describe the bone surface of the HNJ on the 1:00, 1:30, and 2:00 planes, using real bone models rather than simulation models.

There are several possible reasons why our present findings are different from those reported by Uemura *et al.* [12]. The first reason is the difference in the models used; their model was a simulation model and ours was actual human bone models. A second reason is based on the method of analysis. Uemura *et al.* analyzed a 3D surface model of the femur using software, whereas we analyzed in actual roentgen images of bone models. Specifically, we used radiography in the same manner as that used in clinical settings, using the center of the beam and diffusion of the X-rays. We thus speculate that our findings better reflect the clinical situation. A third reason for the discrepant results is the influence of the asphericity of the femoral neck [19]. The femoral head and HNJ were considered spherical in the Uemura study, whereas the present bone model femoral neck's asphericity was likely to influence our results.

In the present study, the ICCs for inter- and intraobserver reliability were "almost perfect agreement" according to the categories suggested by Landis and Koch [17]. In clinical situations,

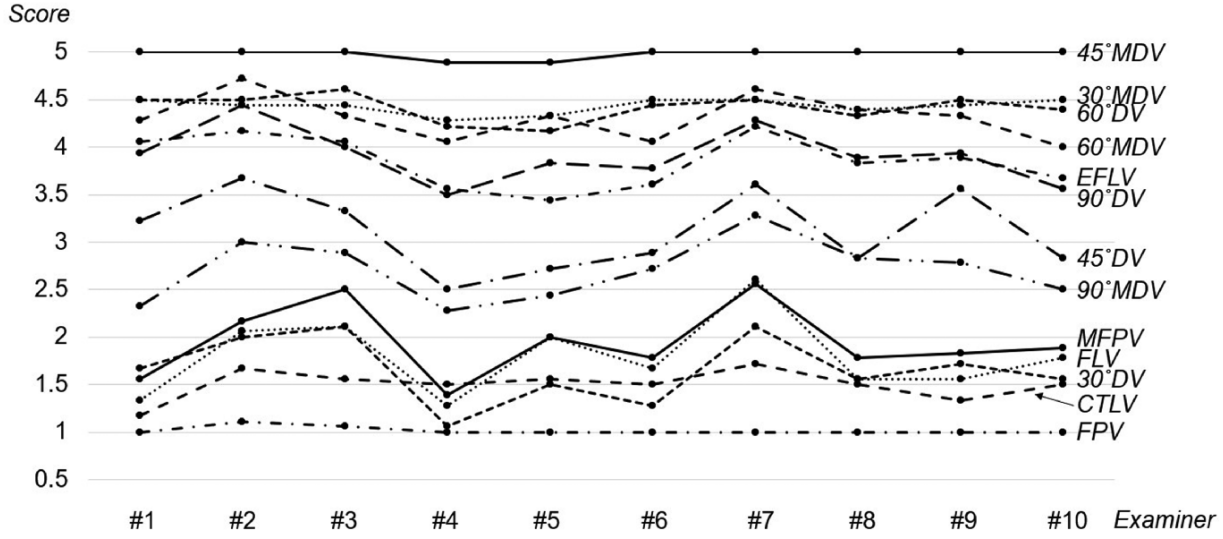

Figure 7. Line graphs showing the examiner's scores on the 1:30 plane. CTLV: cross-table lateral view. The scores are average of 18 measurements, with 3 measurements taken from 6 bone models. The 45° MDV is the best radiographic image and all examiners give the highest score.

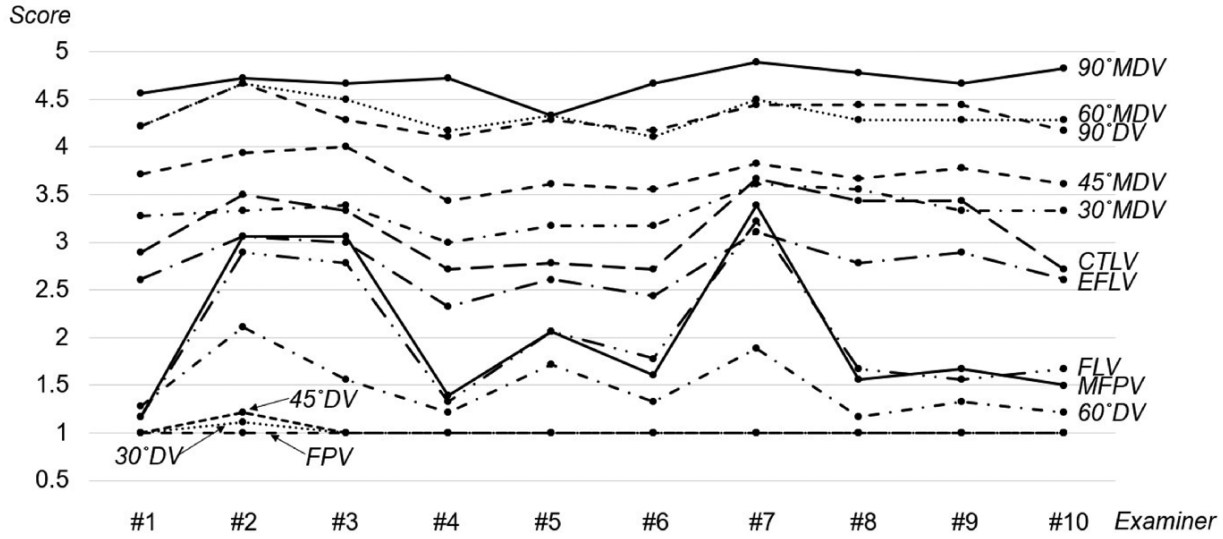

Figure 8. Line graphs showing the examiner's scores on the 2:00 plane. CTLV: cross-table lateral view. The scores are average of 18 measurements, with 3 measurements taken from 6 bone models. The 90° MDV is the best radiographic image. Examiner #5 give the same score as 60° MDV, but the others give the highest score.

if these plain radiographs can accurately evaluate the end-to-end bone surface of the HNJ (i.e. the longitudinal bone surface along the width of the HNJ), we propose that it would be possible to easily evaluate not only the α-angle but also the head–neck offset and/or head–neck offset ratio on the anterosuperior plane, as these are the most important aspects for capturing a cam deformity without subjecting the patient to an additional CT or MRI examination. This method would also be useful for selecting the degree of cam resection using radiographic images for surgery.

There are several study limitations to address. The first limitation was that we could not determine the sex and race of these bone models. There was no mark or list regarding race and sex. However, we speculate and believe that bone models used in the present study were from an Asian population because of the bone morphological features, especially femoral head size. Lin *et al*. reported that the average femoral diameter and the femoral neck-shaft angle were 45.5 mm and 129.9°, respectively, using a 3DCT system on Chinese subjects [20]. In another study, the average femoral neck anteversion evaluated from the transcondylar plane on CT axial images was approximately 15° in Chinese subjects [21]. In Japanese subjects, the average α-angle and head neck offset ratio in the 1:30 CT radial plane were 48.5° and 0.16, respectively [5]. We thus believe that the bone models used in the present study provided normal alignment of the femoral neck and morphology of the HNJ as an Asian population.

The second limitation of this study was that only six bone models were used. The statistical comparison between the best and the second-best radiographies using the average scores

Table 6. The intraobserver reliabilities evaluated by a representative model (bone model #1).

Examiner:	#1	#2	#3	#4	#5	#6	#7	#8	#9	#10
2:00 o'clock plane	0.992	0.996	0.978	0.996	0.989	0.978	0.972	0.982	0.989	0.992
1:30 o'clock plane	0.978	0.979	0.980	0.963	0.977	0.958	0.934	0.934	0.965	0.977
1:00 o'clock plane	0.990	0.976	0.994	0.990	0.960	0.990	0.989	0.978	0.982	1.000

Table 7. The interobserver reliabilities evaluated by a representative model (model #1).

	First examination	Second examination	Third examination
2:00 o'clock plane	0.994	0.992	0.994
1:30 o'clock plane	0.982	0.984	0.986
1:00 o'clock plane	0.994	0.994	0.994

obtained for each bone model did not yield significant results. In some bone models on 2:00 plane, the radiograph having the highest score differed from the radiograph that ranked first overall, suggesting non-negligible variation in HNJ morphology. Based on the present results, it is necessary to determine in advance the number of bone models needed for statistical comparisons in the future studies.

As a third study limitation, there was a possibility of ambiguity in evaluating the scores since the stainless wire markers were 0.45 mm thick, and it is possible that we could not clearly evaluate the differences among the radiographic images. In other words, if a stainless wire marker was shown as an "almost 100% match" to the bone surface, it was impossible to judge whether the stainless wire marker was slightly above the bone surface or slightly below the bone surface in each radial plane. We suspect that there might be ambiguity regarding the differences in the accuracy evaluation because we subjectively evaluated the entire length of the markers, which was ∼22.5 mm in average of our models, attached at the bone surface from the middle point of the femoral neck to the central level of the femoral head.

Finally, each abduction, rotation, and flexion angle differed from those observed in clinical settings. In this investigation, we directly measured each angle using the femoral bone model, whereas in clinical situations, each angle is usually determined based on the thigh, leg, and foot positions, and the rotation angle, in particular, is normally determined using the direction of the foot and leg. Therefore, regarding the 45° DV, 45° MDV, and 90° MDV that we proposed, we believe that it is necessary to have some kind of devices or tools in the X-ray room that accurately reproduces these radiographic limb positions. Additionally, when positioning the lower limbs of obese individuals, it is expected that there will be a significant amount of soft tissue in the direction of imaging. Therefore, we believe it is necessary to create a protocol for imaging conditions for obese patients and create an environment in which they can systematically perform imaging. However, we propose that if the radiography in a clinical setting is performed with the femoral angle maintained correctly like the present study, plain radiography can accurately describe specific planes of the HNJ.

In conclusion, on these bone model studies, the most suitable plain radiography for describing the HNJ at the 1:00, 1:30, and 2:00 planes was the 45° DV, the 45° MDV, and the 90° MDV, respectively.

ACKNOWLEDGEMENTS

We specially thank Division of Anatomy and Cell Biology, Department of Anatomy, Shiga University of Medical Science for supplying human bone models. We also thank Junpei Fujimura, Youko Fujimoto, and Yukinori Tokuda, who are radiological technologist in the Hino Memorial Hospital for performing radiography and CT examination. Finally, we specially thank Jun Matsubayashi from Center for Clinical Research and Advanced Medicine in Shiga University of Medical Science for providing statistical advice.

CONFLICT OF INTEREST

None declared.

FUNDING

None declared.

DATA AVAILABILITY

The data underling this article will be shared upon reasonable request to the corresponding author.

REFERENCES

1. Ganz R, Parvisi J, Beck M *et al.* Femoroacetabular impingement: a cause for osteoarthritis of the hip. *Clin Orthop Relat Res* 2003;**417**:112–20.
2. Agricola R, Waarsing JH, Arden NK *et al.* Cam impingement of the hip: a risk for hip osteoarthritis. *Nat Rev Rheumatol* 2013;**9**:630–34.
3. Hack K, Di Primio G, Rakhra K *et al.* Prevalance of cam-type femoroacetabular impingement morphology in asymptomatic volunteers. *J Bone Joint Surg Am* 2010;**92**:2436–44.
4. Ergen FB, Vudali S, Sanverdi E *et al.* CT assessment of asymptomatic hip joints for the background of femoroacetabular impingement morphology. *Diagn Interv Radiol* 2014;**20**:271–76.
5. Mimura T, Kawasaki T, Itakura S *et al.* Prevalence of radiological femoroacetabular impingement in Japanese hip joints: detailed investigation with computed tomography. *J Orthop Sci* 2015;**20**:649–56.
6. Atkins PR, Shin Y, Agrawal P *et al.* Which two-dimensional radiographic measurements of cam femoroacetabular impingement best describe the three-dimensional shape of the proximal femur? *Clin Orthop Relat Res* 2019;**477**:242–53.
7. Ross JR, Bedi A, Stone RM *et al.* Intraoperative fluoroscopic imaging to treat cam deformities: correlation with 3-dimensional computed tomography. *Am J Sports Med* 2014;**42**:1370–76.

8. Rakhra KS, Sheikh AM, Allen D *et al*. Comparison of MRI alpha angle measurement planes in femoroacetabular impingement. *Clin Orthop Relat Res* 2009;**467**:660–65.
9. Harris MD, Kapron AL, Peter CL *et al*. Correlations between the alpha angle and femoral head asphericity: implications and recommendations for the diagnosis of cam femoroacetabular impingement. *Eur J Radiol* 2014;**83**:788–96.
10. Atkins PR, Kobayashi EF, Anderson AE *et al*. Modified false-profile radiograph of the hip provides better visualization of the anterosuperior femoral head-neck junction. *Arthroscopy* 2018;**34**:1236–43.
11. Uemura K, Atkins PR, Anderson AE *et al*. Do your routine radiographs to diagnose cam femoroacetabular impingement visualize the region of the femoral head-neck junction you intended? *Arthroscopy* 2019;**35**:1796–806.
12. Mimura T, Mori K, Itakura S *et al*. Prevalence of pincer, cam, and combined deformities in Japanese hip joints evaluated with the Japanese Hip Society diagnostic guideline for femoroacetabular impingement: a CT-based study. *J Orthop Sci* 2017;**22**:105–11.
13. Espié A, Chaput B, Murgier J *et al*. 45-45-30 Frog-leg radiograph for diagnosing cam-type anterior femoroacetabular impingement: reproducibility and thresholds. *Orthop Traumatol Surg Res* 2014;**100**:843–48.
14. Clohisy JC, Carlisle JC, Beaulé PE *et al*. A systematic approach to the plain radiographic evaluation of the young adult hip. *J Bone Joint Surg Am* 2008;**90 Suppl 4**:47–66.
15. Dunn DM, Notley B. Anteversion of the neck of the femur; a method of measurement. *Bone Joint Surg Br* 1952;**34–B**:181–86.
16. Lequesne M, De SEZE . False profile of the pelvis. A new radiographic incidence for the study of the hip. Its use in dysplasias and different coxopathies. *Rev Rheum Mal Osteoartic* 1961;**28**:643–52.
17. Landis JR, Koch GG. The measurement of observer agreement for categorical data. *Biometrics* 1977;**33**:159–74.
18. Hellman MD, Mascarenhas R, Gupta A *et al*. The false-profile view may be used to identify cam morphology. *Arthroscopy* 2015;**31**:1728–32.
19. Sugano N, Noble PC, Kamaric E. A comparison of alternative methods of measuring femoral anteversion. *J Comput Assist Tomogr* 1998;**22**:610–14.
20. Lin KJ, Wei HW, Lin KP *et al*. Proximal femoral morphology and the relevance to design of anatomically precontoured plates: a study of the Chinese population. *Sci World J* 2014;**2014**:106941.
21. Hoaglund FT, Low WD. Anatomy of the femoral neck and head, with comparative data from Caucasians and Hong Kong Chinese. *Clin Orthop Relat Res* 1980;**152**:10–16.